CHEMISTRY
A EUROPEAN JOURNAL

DOI: 10.1002/chem.200601561

An Experimental and Computational Study on Intramolecular Charge Transfer: A Tetrathiafulvalene-Fused Dipyridophenazine Molecule

Chunyang Jia,[a, e] Shi-Xia Liu,*[a] Christian Tanner,[a] Claudia Leiggener,[b] Antonia Neels,[c] Lionel Sanguinet,[d] Eric Levillain,[d] Samuel Leutwyler,[a] Andreas Hauser,[b] and Silvio Decurtins[a]

Abstract: To study the electronic interactions in donor–acceptor (D–A) ensembles, D and A fragments are coupled in a single molecule. Specifically, a tetrathiafulvalene (TTF)-fused dipyrido[3,2-*a*:2′,3′-*c*]phenazine (dppz) compound having inherent redox centers has been synthesized and structurally characterized. Its electronic absorption, fluorescence emission, photoinduced intramolecular charge transfer, and electrochemical behavior have been investigated. The observed electronic properties are explained on the basis of density functional theory.

Keywords: charge transfer · donor–acceptor systems · nitrogen heterocycles · photophysical properties · tetrathiafulvalene

Introduction

Heterocycles form by far the largest class of organic compounds and they are of immense importance both industrially and biologically. More specifically, organic compounds possessing a high degree of conjugation are ideal materials for advanced electronic applications in the emerging field of "molecular electronics".[1] Within this context, we set ourselves the synthetic task to fuse together two prominent prototypes of heterocyclic compounds, namely, tetrathiafulvalene (TTF) and dipyrido[3,2-*a*:2′,3′-*c*]phenazine (dppz); each of these units already exhibits on its own a rich and diverse chemistry. Consequently, an efficient approach to a new organic π-conjugated D–A molecule with a metal-chelating diimine functionality has been developed.

Since the discovery of the first organic conductor TTFCl in 1972,[2] TTF has been among the most studied heterocyclic systems.[3] Owing to their unique π-donor properties, TTF and its derivatives are successfully used as versatile building blocks for charge-transfer salts, giving rise to organic conductors and superconductors.[3,4] On the one hand, π-extended TTFs have been investigated to design superior electronic donors with reduced on-site Coulombic repulsion and increased dimensionality.[5] On the other hand, TTFs are frequently used as donor units in D–A ensembles that are of prime interest on account of their potential applications in molecular electronics and optoelectronics.[6] However, only a few examples of TTF-fused D–A systems have been reported in the literature so far, for example, TTF-diquinone[7] and TTF-annulated phthalocyanines.[8] In the former, an intramolecular electron transfer between two quinone groups mediated by a TTF bridge in a purely organic, mixed-valence system has been demonstrated.[7] In the latter, the intramolecular through-bond electronic interactions among TTF moieties were electrochemically evidenced.[8] For more information on conjugated TTF–acceptor systems, the reader may consult a recent review by Wudl et al.[6a]

[a] Prof. Dr. C. Jia, Dr. S.-X. Liu, Dr. C. Tanner, Prof. Dr. S. Leutwyler, Prof. Dr. S. Decurtins
Departement für Chemie und Biochemie
Universität Bern
Freiestrasse 3, 3012 Bern (Switzerland)
Fax: (+41) 31-631-3995
E-mail: liu@iac.unibe.ch

[b] Dr. C. Leiggener, Prof. Dr. A. Hauser
Département de chimie physique, Université de Genève
30 quai Ernest-Ansermet, 1211 Genève 4 (Switzerland)

[c] Dr. A. Neels
Institut de Microtechnique, Université de Neuchâtel
Rue Jaquet-Droz 1, Case postale 526, 2002 Neuchâtel (Switzerland)

[d] Dr. L. Sanguinet, Dr. E. Levillain
Chimie, Ingénierie Moléculaire et Matériaux d'Angers, UMR 6200 du CNRS
2 bd Lavoisier, 49045 Angers Cedex (France)

[e] Prof. Dr. C. Jia
Present address: State Key Laboratory of Electronic Thin Films and Integrated Devices
University of Electronic Science and Technology of China
Chengdu 610054 (China)

Supporting information for this article is available on the WWW under http://www.chemeurj.org/ or from the author.

The interest in the extended dppz compound stems from its fascinating features that include structural planarity, π-extended conjugation, and its metal-chelating diimine functionality.[9] It has been demonstrated that metal complexes containing a dppz ligand, in particular those of ruthenium(II), are good metallointercalators.[10] Furthermore, the luminescence properties of dppz-based complexes have led to their application as DNA "light switches" and probes for long-range DNA-mediated electron-transfer studies.[11] In addition, a recent report by Kelly et al. highlights its specific photochemical behavior.[12]

The herein reported novel organic compound TTF–dppz (**1**), which emerges from the annulation of sulfur- and nitrogen-containing polycycles, allows a thorough experimental and theoretical study of photoinduced charge transfer (CT) in a single D–A molecule. In fact, this transfer occurs between spatially separated electron-rich and electron-deficient fragments within the extended polycyclic system. The present study contrasts and complements a large number of investigations on conjugated systems in which terminal donor and acceptor groups are linked by π-spacers such as oligo(phenylene ethynylene), oligo(phenylene vinylene), and oligothiophene.[13–15] Thereby, the aim is to understand the efficiency of electronic conduction through molecular-scale "wires" as function of distances, geometric conformational changes, and conjugated pathways. It is worth noting that such D–A systems play a crucial role in the development of nonlinear optical materials[16] and in an approach to high-efficiency solar energy conversion.[17]

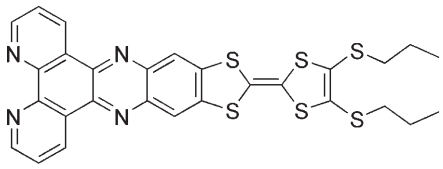

1

Herein, we describe the synthesis and structure of the TTF–dppz molecule (**1**) and examine its electrochemical, optical absorption, photoinduced intramolecular charge-transfer, and fluorescence characteristics. The photophysical properties are rationalized on the basis of density functional theory.

Results and Discussion

Synthesis and characterization: The synthetic pathway is outlined in Scheme 1. The target compound **1** was obtained by direct condensation of 1,10-phenanthroline-5,6-dione with the diamine precursor **3**. The latter was prepared by a phosphite-mediated crosscoupling reaction of 4,5-bis(propylthio)-1,3-dithiole-2-one with **2**, the synthesis of which was based on the known compound 1,2-diamino-benzene-4,5-bis(thiocyanate). All compounds were easily purified by chromatographic separation and have been fully characterized.

Solid-state structure: An ORTEP[18] drawing of **1** is shown in Figure 1. The molecule **1** crystallizes as solvated compound $\mathbf{1}\cdot(CH_2Cl_2)_{0.5}\cdot C_2H_5OH$ in a centrosymmetric orthorhombic space group (*Pbca*). The dark colored crystals have a rod-shaped morphology, in which the *a* axis lies parallel to the rod axis. The asymmetric unit comprises the complete molecule, thus all atoms lie on general positions. The skeleton of the molecule is virtually planar; the rms deviation from a least-squares plane through all atoms, excluding the two peripheral propyl groups, is 0.050 Å. Similarly, a least-squares plane through the atoms of the TTF core alone reveals a rms deviation of only 0.027 Å. The bond lengths in

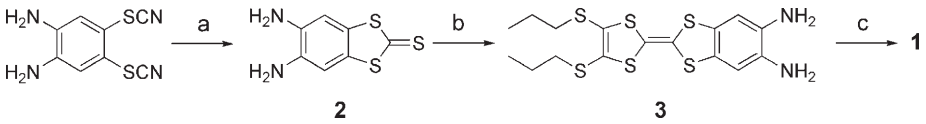

2 **3**

Scheme 1. Reagents and conditions: a) $Na_2S\cdot 9H_2O$ (3.3 equiv), CS_2 (2.1 equiv), H_2O, 50 °C, 52 %; b) 4,5-bis-(propylthio)-1,3-dithiole-2-one (2 equiv), triethylphosphite/toluene, 120 °C, 37 %; c) 1,10-phenanthroline-5,6-dione (1 equiv), ethanol, refluxed, 65 %.

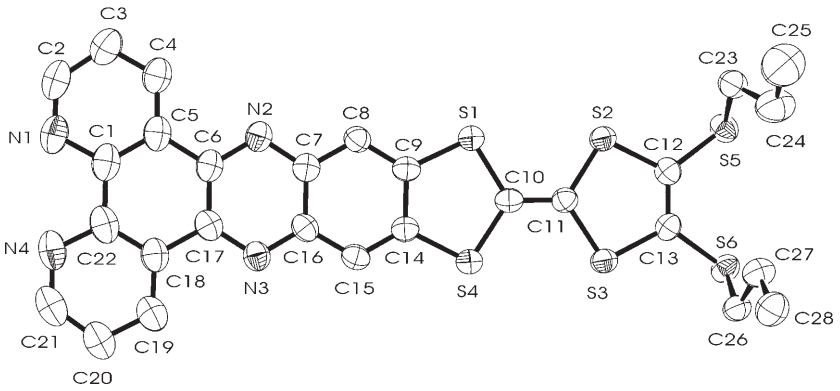

Figure 1. ORTEP view of the molecule **1**. Hydrogen atoms and solvent molecules have been omitted for clarity. Selected interatomic distances [Å] and bond angles [°]: C10–C11 1.345(6), C10–S1 1.748(4), C10–S4 1.756(4), C11–S2 1.745(4), C11–S3 1.755(4), C9–C14 1.440(5), C12–C13 1.344(6); S1-C10-S4 115.7(3), S2-C11-S3 114.4(2), C7-N2-C6 116.0(4), C16-N3-C17 116.8(4), C11-C10-S1 121.2(3), C11-C10-S4 123.0(3), C10-C11-S3 123.1(3), C10-C11-S2 122.4(3).

the TTF moiety are in the range expected for neutral TTF derivatives[19] and similarly, the distances of the dppz unit span the expected range in comparison with literature values.[20] Figure 2 highlights the mutual arrangement of the molecules in the crystal structure. A noticeable feature is the parallel head-to-head alignment with intermolecular S···S contacts of 3.524 Å and 3.657 Å.

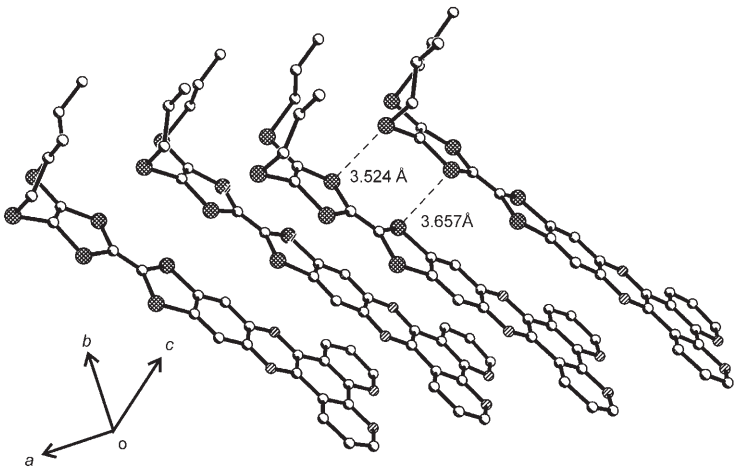

Figure 2. View of the crystal packing arrangement of **1**. Hydrogen atoms and solvent molecules have been omitted for clarity.

Electrochemistry: The electrochemical properties of TTF–dppz conjugate **1** and its precursor **3** in dichloromethane were investigated by cyclic voltammetry (CV) and thin-layer cyclic voltammetry (TLCV). Their electrochemical data are collected in Table 1 together with those of TTF for comparison. Compound **3** shows two reversible single-electron oxidation waves, typical of the TTF system corresponding to $E_{1/2}^{ox1}$ and $E_{1/2}^{ox2}$ in Table 1. In the case of **1**, several CV experiments were performed at different scan rates (Figure 3). The results indicated that the second oxidation process, from the radical cation to the dication species, is not electrochemically reversible, especially at low scan rates, while the first one is reversible. This effect is enhanced under TLCV conditions: the intensity of the reduction of the dication decreases progressively as the potential is cycled (Figure 4, top). Hence, the instability of the dication in the vicinity of the working electrode is probably attributable to a cleavage of the conjugation between the TTF^{2+} moiety and the dppz unit.

Table 1. Redox potentials (V versus Ag/AgCl) of compounds **1** and **3** as well as TTF.[21]

Compound	$E_{1/2}^{ox1}$	$E_{1/2}^{ox2}$	$E_{1/2}^{red}$
1	0.73	1.08	−1.17
3	0.36	0.73	
TTF	0.41	0.71	

The redox potentials are quite sensitive to the substituent groups of the TTF core. Compared to those of TTF, the potential values of **1** and **3** show a positive and a negative shift, probably attributable to an electron-withdrawing effect of the phenazine group and the electron-donating ability of NH_2 units, respectively. In addition, TTF–dppz conjugate **1** undergoes a reversible one-electron reduction process, which can be assigned to reduction of the phenazine moiety (Figure 4, bottom).

Photophysical properties and ab initio calculations

*The neutral TTF-dppz conjugate (**1**)*: The UV-visible-NIR spectrum of **1** dissolved in CH_2Cl_2 (Figure 5) shows a strong absorption band at 26800 cm^{-1} with a shoulder, and a broad band in the visible centered at 18500 cm^{-1} with an oscillator strength of 0.17. While dppz and the TTF analogue of **3** with CN groups instead of the NH_2 groups also exhibit absorption bands above 20000 cm^{-1} (see the Supporting Information), the band at 18500 cm^{-1} is only observed in the fused TTF–dppz. In addition, compound **1** shows fluorescence in solution at room temperature. As depicted in Figure 6, and in contrast to the absorption spectrum, the fluorescence spectrum is strongly solvent-dependent. It shifts monotonically to the red with increasing polarity of the seven solvents given in Table 2, which summarizes the relevant spectro-

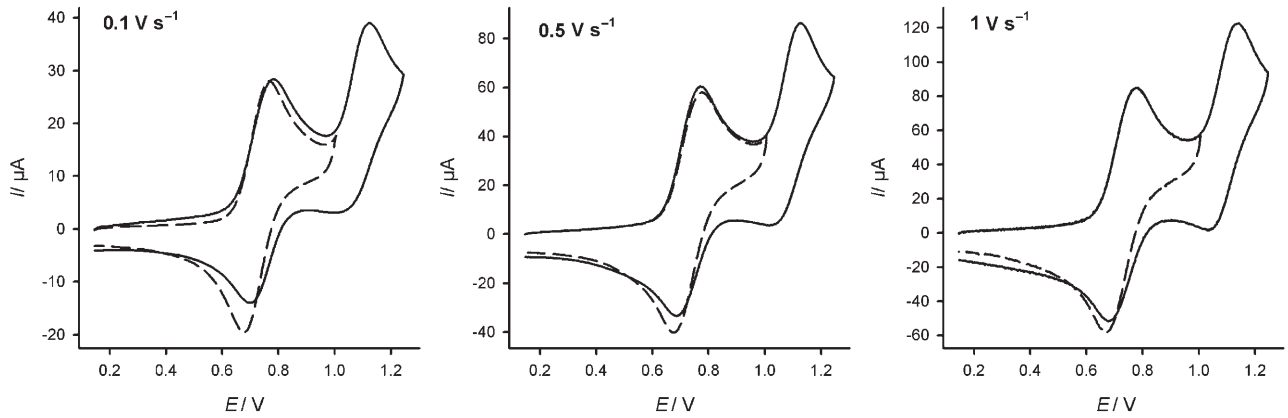

Figure 3. Cyclic voltammograms of **1** in CH_2Cl_2 to the monocation (dashed line) and to the dication (solid line) at different scan rates, V versus Ag/AgCl.

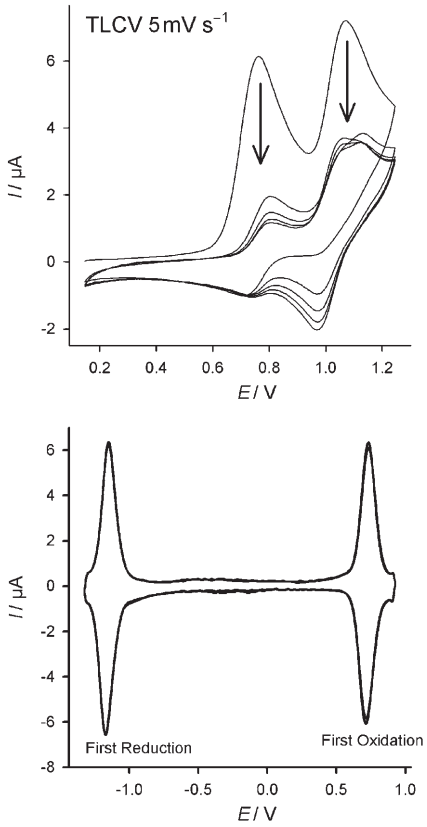

Figure 4. TLCV of **1** in CH_2Cl_2 at 5 mV s^{-1}: in the positive direction with cycling in potential (top) and to the radical cation and to the radical anion, *V* versus Ag/AgCl (bottom).

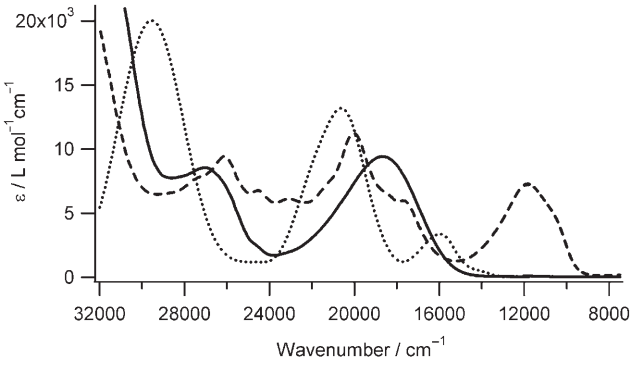

Figure 5. Absorption spectra of the TTF-dppz conjugate in CH_2Cl_2 at room temperature. Neutral form (**1**) (——), radical cation (**1**$^+$) (-----), and anion (**1**$^-$) (•••••). The radical cation was obtained by chemical oxidation of **1** by $[Fe(bpy)_3]^{3+}$ and the spectrum was corrected for the absorption from the reduced oxidizing agent, namely from the intense MLCT band of $[Fe(bpy)_3]^{2+}$. The anion was produced electrochemically.

scopic results. In parallel, the fluorescence quantum yield at room temperature decreases from 7.6% in cyclohexane to 0.1% in DMF. As shown in Figure 6, the excitation spectrum of **1** is identical to its absorption spectrum, and indeed such is the case for all solvents of the series.

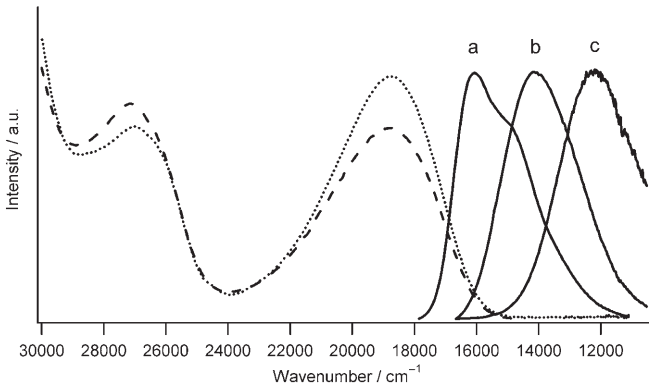

Figure 6. Emission spectra (——, $\nu_{ex}=18518$ cm^{-1}, $\lambda_{ex}=540$ nm) of the TTF-dppz conjugate (**1**) in different solvents at room temperature, a) cyclohexane, b) toluene, c) dichloromethane, and absorption (•••••) and excitation spectra (-----, $\nu_{em}=13888$ cm^{-1}, $\lambda_{em}=720$ nm) of **1** in toluene.

Table 2. Absorption and emission maxima, A_{max} and E_{max} respectively, Stokes shift ν_{ST}, and luminescence quantum yield Φ_F of the TTF–dppz conjugate in different solvents. Δf is the corresponding solvent polarity parameter.

Solvent	Δf	A_{max} [cm^{-1}]	E_{max} [cm^{-1}]	ν_{ST} [cm^{-1}]	Φ_F
DMF	0.275	19304	11571	7733	0.0013
acetone	0.284	19121	11645	7476	0.001
CH_2Cl_2	0.228	18690	12198	6492	0.01
THF	0.210	18978	12690	6288	0.0072
$CHCl_3$	0.149	18284	12531	5753	0.012
toluene	−0.004	18622	14124	4498	0.063
cyclohexane	−0.001	18551	16077	2474	0.076

The fluorescence of **1** is significantly different from that of dppz, which has a maximum at 23900 cm^{-1} (see the Supporting Information). This, together with the excellent agreement between absorption and excitation spectra, proves that the fluorescence is indeed attributable to TTF–dppz and not to an impurity or a photoproduct. The fluorescence lifetime in CH_2Cl_2 is 0.4 ns, which, together with the quantum yield of ≈1% at room temperature, results in a radiative lifetime (τ_{rad}) of 40 ns. This value is in excellent agreement with τ_{rad} estimated from the oscillator strength of the absorption band at 18500 cm^{-1}. Moreover, and quite remarkably, the CT energy calculated from the electrochemical data in Table 1 is 1.9 eV (or 15320 cm^{-1}), which is almost the same as the energy of the CT excited state evaluated from the crossing-point of the absorption and fluorescence spectra (15350 cm^{-1}).

The solvent dependence of the fluorescence indicates that the excited state is stabilized in more polar solvents, as expected for an intramolecular CT. To obtain more information about the change in the dipole moment upon excitation, we use the Lippert–Mataga equation [Eq. (1)],[22,23] which expresses the Stokes shift as a function of the solvent polarity parameter Δf

$$\nu_{ST} = 2\,(\mu_e-\mu_g)^2\,\frac{\Delta f}{hca^3} + C = 10070\,(\mu_e-\mu_g)^2\,\frac{\Delta f}{a^3} + C \qquad (1)$$

where Δf is calculated from Equation (2):[22]

$$\Delta f = \frac{(\varepsilon-1)}{(2\varepsilon+1)} - \frac{(n^2-1)}{(2n^2+1)} \quad (2)$$

and ε and n are the dielectric constant and the refractive index of the solvent, respectively. The Δf values for the series of solvents are included in Table 2. In Equation (1), μ_e and μ_g are the dipole moments of the excited state and the ground state respectively, h is Planck's constant, c is the velocity of light and a is the Onsager radius. The latter is set to 5.7 Å, as estimated from the crystallographic molecular volume of **1**, projected onto a sphere of the same volume. For the dipole moments in Debye and a in Å, the prefactor $2/(hc) = 10070$.[24] The Lippert–Mataga plot for TTF–dppz conjugate **1** is shown in Figure 7. From the slope of this plot, the difference of the dipole moment between the excited state and the ground state is estimated to be 16 Debye. This large change in dipole moment upon excitation is typical for photoinduced intramolecular CT processes.

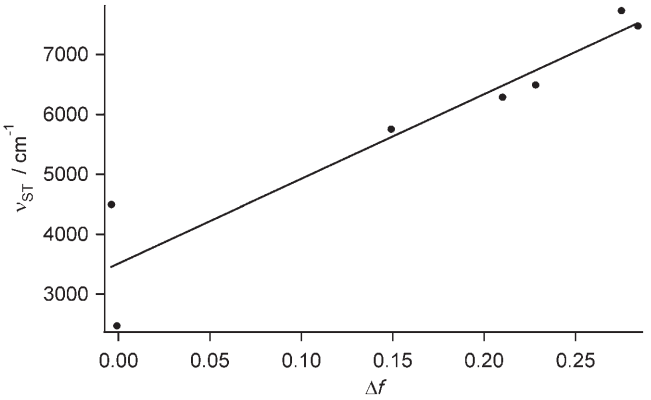

Figure 7. Lippert–Mataga plot for the TTF–dppz conjugate (**1**).

The key question to be answered in the following regards the nature of the CT character of the absorption band centered at 18500 cm^{-1}. In the crystal, the structure of **1** is close to planar with only the thioalkyl groups oriented nearly orthogonally to the molecular plane. However, the gas-phase structure, optimized with the above-mentioned computational methods, is distinctly nonplanar with a 37° bend at the inner S atoms of the tetrathiafulvalene unit. A similar boat-type distortion has also been predicted for the TTF subunit.[25] Upon oxidation, the gas-phase structure of $\mathbf{1}^+$ reverts to near-planarity, the same as that calculated for TTF^+.[25] Owing to the minimal energy differences between the different forms, only the C_s symmetric structure of **1** and the C_2 symmetric structure of $\mathbf{1}^+$ are discussed below. In a room-temperature solution, all these structures will be populated.

To rationalize the electronic absorption spectrum of **1**, configuration interaction singles (CIS) and time-dependent density functional (TDDFT) calculations with the B3LYP functional were performed for the low-lying excited states. Vertical excitations were calculated at the optimized C_s ground-state geometry. Overall, the CIS calculations qualitatively agree with the TDDFT calculations; however, their predictions of the electronic transitions are systematically too high in energy. At the TDDFT level, the lowest-energy singlet transition of **1** is calculated to be an allowed in-plane π–π^* transition with an oscillator strength $f_{calcd} = 0.282$. The transition is predicted to be at 2.19 eV (17630 cm^{-1}), in excellent agreement with the lowest-energy band of the absorption spectrum at 18500 cm^{-1} (Table 3). This excitation corresponds essentially to a one-electron HOMO→LUMO excitation. The HOMO of **1** is a π orbital centered on the TTF subunit, designated in Figure 8 as orbital #141. In contrast, the LUMO of **1** (#142) is centered on the phenazine subunit of the dppz moiety and closely corresponds to the LUMO of bare phenazine. Therefore, the lowest-energy transition corresponds to an intramolecular CT transition from the TTF as a donor unit to the dppz as an acceptor unit. The charge flow along the molecule associated with this intramolecular CT transition is very large: the dipole moment calculated at the HF/6-31+G(d,p) level is only 0.9 D in the S_0 state, increasing to 5.9 D in the S_1 state. The detailed charge redistribution upon $S_0 \rightarrow S_1$ electronic excitation, calculated at the CIS/6-31+G(d,p) level, is depicted in Figure 8: the TTF unit (including the thioalkyl groups) loses electron density which is transferred to the phenazine subunit. Although the experimental change in the dipole moment derived from the Lippert–Mataga equation is considerably larger than that calculated, we consider that the calculation supports the experimental result inasmuch as the

Table 3. Vertical excitations of **1** and $\mathbf{1}^+$ at the time-dependent DFT level of theory [B3LYP and UB3LYP/6-311++G(d,p)].

Excited state	One-electron excitation	Oscillator strength	Transition energy [cm^{-1}]	Experimental transition energy [cm^{-1}]
		1 (C_s)		
$1^1A'$	141→142	0.282	17630	18500
$2^1A'$	141→145	0.001	24100	
$1^1A''$	141→143	0.008	24860	
$2^1A''$	140→142	0.015	25700	
$3^1A'$	141→144	0.000	26650	
$4A'$	139→142	0.239	26800	26 800
		$\mathbf{1}^+$ (C_2)		
1^2B	140β→141β	0.000	8080	
1^2A	139β→141β	0.000	8950	
2^2A	138β→141β	0.297	11260	11800
2^2B	137β→141β	0.000	12560	
3^2B	136β→141β	0.001	13350	
3^2A	134β→141β	0.004	14020	
4^2B	135β→141β	0.000	14260	
5^2B	133β→141β	0.000	15140	
6^2B	139α→142α	0.000	18410	
7^2B	132β→141β	0.008	19610	
4^2A	130β→141β	0.109	19890	17600
5^2A	141α→142α	0.125	21110	20000

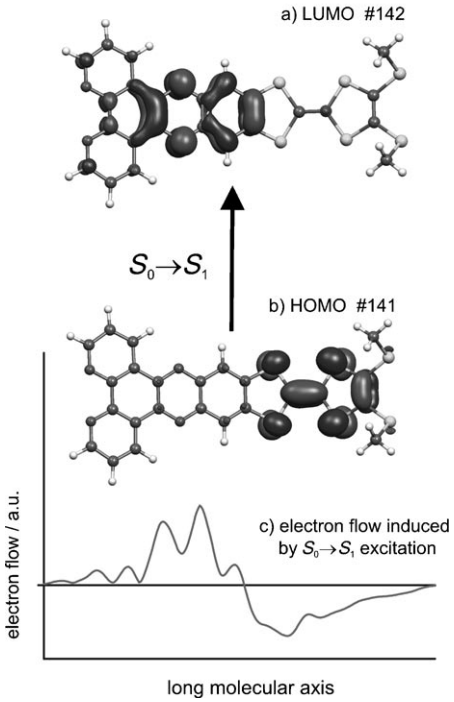

Figure 8. The $S_0 \rightarrow S_1$ transition of **1** essentially corresponds to a single-electron HOMO→LUMO excitation. The charge flow diagram illustrates the charge-transfer character of this transition.

Lippert–Mataga equation is notorious for overestimating dipole moment changes.

The observed fluorescence in the red and near-IR region can only be assigned to the $S_1 \rightarrow S_0$ CT emission. The associated solvent-dependent Stokes shifts imply 1) an extensive intramolecular geometry change accompanying the $S_1 \rightarrow S_0$ transition and 2) reorientation of the solvent molecules in the vicinity of the TTF–dppz solute, following the charge rearrangement in the molecule. Both effects are expected to be substantial. Indeed, upon the $S_0 \rightarrow S_1$ charge-transfer excitation the TTF unit shows a calculated increase of 0.06 Å for the central C–C double bond and a 0.04 Å decrease of the four C–S bond lengths, rather similar to the ground-state geometry changes between TTF and TTF^+.[25]

The next $S_0 \rightarrow S_n$ absorptions of **1** are predicted to be weak. The second intense transition (Figure 5) is assigned to $S_0 \rightarrow S_6$, corresponding to the HOMO–LUMO transition of the dppz moiety. It is calculated to lie at 3.32 eV (26800 cm^{-1}) with roughly the same intensity ($f_{calcd} = 0.239$) as the $S_0 \rightarrow S_1$ transition. This is also in very good agreement with the observed absorption band at 26800 cm^{-1} ($\varepsilon =$ 8000 $L\,mol^{-1}\,cm^{-1}$).

Coordination to metal ions: The dppz unit provides a suitable coordination site for cations such as Fe^{2+}, Zn^{2+}, and Ru^{2+}. Upon addition of Fe^{2+} or Zn^{2+}, for instance, the TTF-dppz solution changes color from purple to blue. The color change is purely due to a red-shift of the CT band by $\Delta E \approx 2000\ cm^{-1}$, as shown in Figure 9 for the Zn^{2+}-coordinated compound. The spectrum of the Fe^{2+}-coordinated TTF–dppz is almost identical. The coordination of a metal ion at the phen site reduces the electron density on the aromatic ring system, thereby lowering the energy of the LUMO. As a result, the corresponding spectroscopic TTF→dppz CT transition moves to lower energies. The fact that the shift of the CT band is nearly identical for coordination to Zn^{2+} and Fe^{2+} shows that the effect is of an essentially electrostatic nature. However, there is a difference in the luminescence properties. As shown in Figure 9, the luminescence of Zn^{2+}-coordinated TTF-dppz is red-shifted as well and the intensity drops to ≈20% of the intensity of non-coordinated TTF–dppz. In the case of Fe^{2+}-coordinated TTF–dppz, the luminescence is completely quenched. Whereas the reduced quantum yield for the Zn^{2+} complex is attributed to the smaller energy gap and to the resulting increase in the radiationless decay according to the energy gap law in the Marcus inverted region, in the case of the Fe^{2+} complex, the low-lying ligand field states provide an efficient ladder for non-radiative decay. Protonation of the nitrogen atoms of the phen unit using formic acid results in a similar red shift of the CT transition and quenches the luminescence to about 5% of the original intensity.

*Oxidation of the TTF-dppz conjugate (**1**):* Compound **1** can be chemically oxidized to its radical cation $\mathbf{1}^+$ by $[Fe(bpy)_3]^{3+}$. The decrease of the CT band at 18500 cm^{-1} upon oxidation occurs simultaneously with the appearance of new absorptions at 11800 cm^{-1} and 17600/20000 cm^{-1}, as shown in Figure 5. Similar absorption bands have been observed after oxidation of the above-mentioned TTF reference compound (see the Supporting Information).

The spin-unrestricted UB3LYP TDDFT calculations for the open-shell $\mathbf{1}^+$ cation predict the two lowest-energy tran-

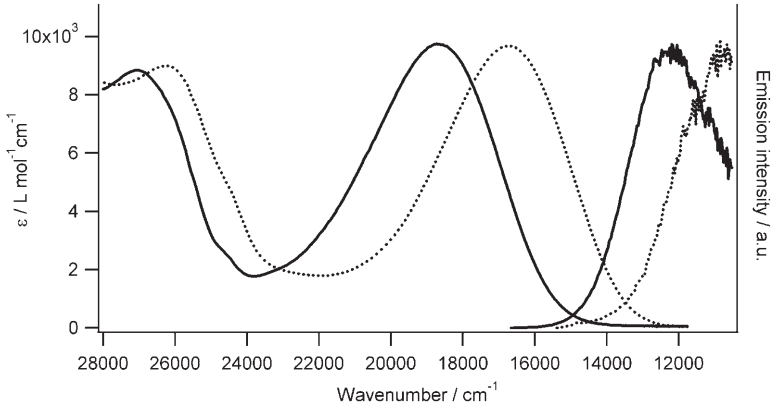

Figure 9. Absorption and emission spectra of **1** in CH_2Cl_2 before (——) and after addition of Zn^{2+} (-----). The emission spectra were scaled to the same height.

sitions of $\mathbf{1}^+$ to be very weak or even zero (Table 3). The third ($D_0 \rightarrow D_3$) transition is calculated to be an intense band in the near-IR at 11260 cm^{-1} with $f_{calc} = 0.297$. This agrees very well with the observed band at 11800 cm^{-1}. The character of this transition is again an intramolecular CT; however, it is in the opposite direction to that of the neutral compound **1**: for $\mathbf{1}^+$ it is dominated by a one-electron excitation from orbital #138 (SOMO-3), which is largely localized on dppz, to the SOMO (#141) that is localized on TTF (Figure 10). The next few $D_0 \rightarrow D_n$ absorptions are again predicted to be very weak or zero. The strong absorptions at 17600/20000 cm^{-1} can be assigned to $D_0 \rightarrow D_{11}$ and $D_0 \rightarrow D_{12}$. The former transition is centered on the TTF subunit; the latter is the SOMO→LUMO transition of $\mathbf{1}^+$ and is analogous to the HOMO→LUMO ($S_0 \rightarrow S_1$) transition of **1**. No fluorescence from D_3 is observed, as expected for a higher electronically excited state.

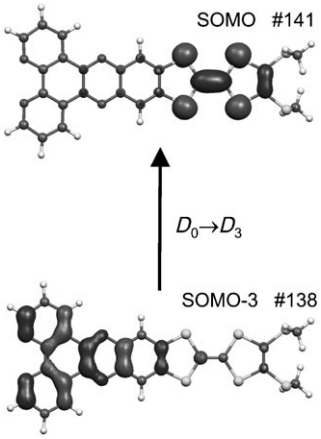

Figure 10. The $D_0 \rightarrow D_3$ transition of $\mathbf{1}^+$ essentially corresponds to the promotion of an electron from the SOMO-3 to the SOMO.

*Reduction of the TTF-dppz conjugate (**1**):* The absorption spectrum of $\mathbf{1}^-$ included in Figure 5 consists of three bands at 29500 cm^{-1} (338 nm), at 20600 cm^{-1} (485 nm), and at 16000 cm^{-1} (626 nm). Upon one-electron reduction of dppz, two new absorption bands at about 330 nm and 580 nm are observed.[26] The spectrum is found to be similar to the singly reduced phenazine (maxima at 375 nm and 551 nm) and therefore the added electron is suggested to be located on the phenazine-based orbital. Thus, in the case of $\mathbf{1}^-$, the absorption bands at 29500 cm^{-1} and at 16000 cm^{-1} are most likely to be attributable to $dppz^-$, while the band at 20600 cm^{-1} is characteristic for fused $(TTF–dppz)^-$, and it can tentatively be assigned to a dppz→TTF CT transition.

Conclusion

During this study, an efficient synthetic route to the important precursor 5,6-diamino-2-(4,5-bis(propylthio)-1,3-dithiole-2-ylidene)-benzo[*d*]-1,3-dithiole (**3**) has been developed. This protocol provides not only a versatile and convenient pathway to new TTF derivatives in good yields and high purity, it also paves the way for the attachment of many functional groups fused to the core of the donor framework.[27] The novel feature of the fused TTF-dppz compound **1** is that it shows fascinating physical properties that are not just given by the sum of the properties of the building blocks. The excited state with the lowest energy corresponds to an intramolecular TTF→dppz CT state. The transition to this state is dipole-allowed and appears as a comparatively strong absorption band in the visible. Remarkably, the corresponding CT fluorescence is also observed, with large solvent-dependent Stokes shifts of 2400–7700 cm^{-1}. The quantum efficiency approaches 0.1, which is unique in view of the fact that fluorescence from D–A diads containing TTF is virtually unknown. We note that the charge recombination associated with the $S_1 \rightarrow S_0$ transition is comparatively slow, up to 3 ns in cyclohexane, estimated from the radiative lifetime of 40 ns and the luminescence quantum yield of 7.6% in this solvent.

The fact that the dppz unit simultaneously serves as ligand for binding metal ions paves the way for devising triad systems that show long-lived light-induced charge separation. The binding of conjugate **1** to a variety of transition metal ions and their excited-state charge separation characteristics are currently under investigation in our laboratory and will be published in due course.

Experimental Section

General methods and materials: Air- and/or water-sensitive reactions were conducted under nitrogen using dry, freshly distilled solvents. Unless stated otherwise, all other reagents were purchased from commercial sources and used without additional purification. 1,2-Diamino-benzene-4,5-bis(thiocyanate),[28] 4,5-bis(propylthio)-1,3-dithiole-2-one,[29] and 1,10-phenanthroline-5,6-dione[30] were prepared according to literature procedures. Elemental analyses were performed on an EA 1110 Elemental Analyzer CHN Carlo Erba Instruments. FT-IR spectra were recorded on a Perkin Elmer One FT-IR spectrometer. Mass spectra were recorded on a Micromass AutoSpec spectrometer using EI.

Cyclic voltammetry: Cyclic voltammetry (CV) was performed in a three-electrode cell equipped with a platinum millielectrode, a platinum wire counter-electrode and a silver wire used as a quasi-reference electrode. The electrochemical experiments were carried out under a dry and oxygen-free atmosphere ($H_2O < 1$ ppm, $O_2 < 1$ ppm) in CH_2Cl_2 (0.8 mM) with Bu_4NPF_6(TBAP) (0.1 M) as the support electrolyte. The voltammograms were recorded on an EGG PAR 273 A potentiostat with positive feedback compensation. Based on repetitive measurements, absolute errors on potentials were estimated to be $\approx \pm 5$ mV. The determination of the number of electrons was performed by recording the voltammograms in thin-layer conditions (TLCV), and dichloronaphthoquinone was used as an internal reference for the number of exchanged electrons. The experimental voltammograms were deconvoluted with CondeconTM software.

Photophysical measurements: Photophysical measurements were performed on degassed solutions of **1** dissolved in CH_2Cl_2 ($c = 2 \times 10^{-5}$ M) and a number of other organic solvents. Absorption spectra were recorded on a Cary 50 Bio UV/Vis spectrophotometer and on a Bruker IFS 66/S NIR spectrophotometer at room temperature. Emission and excitation spectra were measured on a Horiba Fluorolog 3. Fluorescence lifetime measure-

ments ($\lambda_{ex}=480$ nm) were performed on a custom-built time-correlated photon-counting system. Chemical oxidation of compound **1** (in CH_2Cl_2) to the monocation $\mathbf{1}^+$ was achieved by titration with $[Fe(bpy)_3](PF_6)_3$ (in CH_3CN). The oxidation reaction was found to be stoichiometric, that is, the reduction of $[Fe(bpy)_3]^{3+}$ to $[Fe(bpy)_3]^{2+}$ is quantitative. The formation of $[Fe(bpy)_3]^{2+}$ was detected by means of UV/Vis spectroscopy. Reversibility of the chemical oxidation was checked by reduction with ferrocene.

Ab initio calculations: Ab initio calculations of **1** and $\mathbf{1}^+$ in their respective electronic ground states were performed with the Hartree–Fock SCF and B3LYP density functional (DFT) methods and the 6-31+G(d,p) and 6-311++G(d,p) basis sets. The structure of **1** was fully optimized in C_s symmetry with the mirror plane perpendicular to the aromatic plane of the dppz subunit. Related C_{2v}, C_2, and C_1 structures were optimized as well; these lie within a few kcal mol^{-1} of the C_s structure. The structure of $\mathbf{1}^+$ was optimized in C_2 geometry. All calculations were performed with the Gaussian 03 program system.[31]

5,6-Diaminobenzene-1,3-dithiole-2-thione (2): The reported procedure[32] was modified as follows: 1,2-diaminobenzene-4,5-bis(thiocyanate) (2.44 g, 11 mmol) was added to a degassed solution of $Na_2S{\cdot}9H_2O$ (8.71 g, 36 mmol) in water (135 mL), and the mixture was heated to 70 °C for 1 h to produce a clear brownish solution. The mixture was cooled to 50 °C, and CS_2 (1.4 mL, 23.2 mmol) was slowly added dropwise. The mixture was stirred for 2 h at 50 °C and for another 3 h at room temperature. The precipitate was filtered off, washed with water, and air-dried. The crude product was purified by flash column chromatography (silica gel, CH_2Cl_2/EtOAc (1/3, v/v)) to give **2** as a yellow powder (1.21 g, 52 %). M.p. 210–211 °C; ^{1}H NMR (300 MHz, [D$_6$]DMSO): $\delta=6.76$ (s, 2H), 5.07 ppm (s, 4H); ^{13}C NMR (75 MHz,[D$_6$]DMSO): $\delta=210.1$, 136.8, 127.9, 105.4 ppm; IR: $\tilde{\nu}=3384$, 3315, 1621, 1557, 1487, 1293, 1050, 1033, 892 cm^{-1}; MS (EI): *m*/*z* (%): 214 (100) $[M]^+$; elemental analysis (%) calcd for $C_7H_6N_2S_3$: C 39.23, H 2.82, N 13.07; found: C 39.57, H 2.71, N 12.93.

5,6-Diamino-2-(4,5-bis(propylthio)-1,3-dithio-2-ylidene)benzo[*d*]-1,3-dithiole (3): Triethylphosphite (30 mL) was added slowly to a solution of 4,5-bis(propylthio)-1,3-dithiole-2-one (1.24 g, 4.68 mmol) and compound **2** (0.5 g, 2.34 mmol) in toluene (20 mL) under N_2. The mixture was heated to 120 °C and stirred for 3 h. After the reaction, the excess solvent was removed under vacuum to afford an oily red residue, which was subjected to chromatography (silica gel, CH_2Cl_2/EtOAc (1/3, v/v)). The crude product was further purified by recrystallization from CH_2Cl_2/hexane to give compound **3** as a yellow solid (0.37 g, 37 %). M.p. 127–128 °C; ^{1}H NMR (300 MHz, [D$_6$]DMSO): $\delta=6.54$ (s, 2H), 4.69 (s, 4H), 2.78–2.83 (t, 4H), 1.52–1.59 (m, 4H), 0.91–0.96 ppm (t, 6H); ^{13}C NMR (75 MHz,[D$_6$]DMSO): $\delta=134.9$, 126.9, 121.0, 114.3, 107.5, 105.3, 37.3, 22.6,12.7 ppm; IR: $\tilde{\nu}=3392$, 3320, 2960, 1619, 1489, 1292, 854 cm^{-1}; MS (EI): *m*/*z* (%): 432 (44) $[M]^+$; elemental analysis calcd (%) for $C_{16}H_{20}N_2S_6$: C 44.41, H 4.66, N 6.47; found: C 44.68, H 4.67, N 6.33.

4′,5′-Bis(propylthio)tetrathiafulvenyl[*i*]dipyrido[3,2-*a*:2′,3′-*c*]phenazine (1): A solution of compound **3** (100 mg, 0.23 mmol) and 1,10-phenanthroline-5,6-dione (48.3 mg, 0.23 mmol) in ethanol (40 mL) was refluxed for 3 h under N_2. After filtration, the precipitate was collected and purified by chromatography (basic Al_2O_3, CH_2Cl_2/CH_3OH (10/1, v/v)) to give compound **1** as a deep blue powder (91 mg, 65 %). M.p. 238–240 °C; ^{1}H NMR (300 MHz, $CDCl_3$): $\delta=9.42$–9.43 (d, 2H), 9.22–9.23 (d, 2H), 8.0 (s, 2H), 7.72–7.76 (m, 2H), 2.81–2.86 (t, 4H), 1.66–1.73 (m, 4H), 1.01–1.06 ppm (t, 6H); ^{13}C NMR (75 MHz, $CDCl_3$): $\delta=152.4$, 148.1, 143.1, 141.3, 140.6, 133.5, 127.9, 127.3, 124.1, 119.7, 115.6, 107.8, 38.4, 23.2, 13.2 ppm; IR: $\tilde{\nu}=2959$, 1436, 1357, 1090, 741 cm^{-1}; MS (EI): *m*/*z* (%): 606 (8)$[M]^+$; elemental analysis calcd (%) for $C_{28}H_{22}N_4S_6$: C 55.41, H 3.65, N 9.23; found: C 55.15, H 3.47, N 9.26. Single crystals suitable for X-ray analysis were obtained by slow evaporation of a CH_2Cl_2/EtOH solution of **1**.

X-ray structure determination: A black, rod-like crystal of compound **1** was mounted on a Stoe Mark II Imaging Plate Diffractometer System (Stoe & Cie, 2002) equipped with a graphite monochromator; 200 exposures (5 min per exposure) were obtained at an image plate distance of 140 mm, $\phi=0°$ and $0°<\omega<100°$ with the crystal oscillating through 0.5° in ω. The resolution was D_{min}–D_{max} 17.78–0.72 Å. The structure was solved by direct methods using the program SHELXS-97[33] and refined by full-matrix least-squares on F^2 with SHELXL-97.[34] The hydrogen atoms were included in calculated positions and treated as riding atoms using SHELXL-97 default parameters. One dichloromethane molecule having the occupancy of 0.5 is found per asymmetric unit. Two ethanol molecules being partially occupied and strongly disordered are co-crystallized. Therefore, the SQUEEZE instruction in PLATON 03[18] was used to calculate the potential solvent accessible volume in the unit cell; 1567 Å^3 were calculated to contain ≈237 electrons. Therefore, 8 ethanol molecules (8×26 electrons) per unit cell were included in all further calculations. All non-hydrogen atoms were refined anisotropically. A semi-empirical absorption correction was applied using DIFABS (PLATON 03[18] $T_{min}=0.375$, $T_{max}=0.782$). CCDC-626169 (**1**) contains the supplementary crystallographic data for this paper. These data can be obtained free of charge from the Cambridge Crystallographic Data Centre via www.ccdc.cam.ac.uk/data_request/cif.

Acknowledgements

This work was supported by the National Science Foundation (grant No. 200020-107589 and COST Action D31) as well as by the ESF program - SONS (NANOSYN). We thank Eric Vauthey of the University of Geneva for the determination of the luminescence lifetime.

[1] R. L. Carroll, C. B. Gorman, *Angew. Chem.* **2002**, *114*, 4556–4579; *Angew. Chem. Int. Ed.* **2002**, *41*, 4378–4400.
[2] F. Wudl, D. Wobschall, E. Hufnagel, *J. Am. Chem. Soc.* **1972**, *94*, 670–672.
[3] J. Yamada, T. Sugimoto, *TTF Chemistry. Fundamentals and applications of Tetrathiafulvalene*, Springer, Berlin, **2004**.
[4] T. Otsubo, K. Takimiya, *Bull. Chem. Soc. Jpn.* **2004**, *77*, 43–58.
[5] a) M. Iyoda, M. Hasegawa, Y. Miyake, *Chem. Rev.* **2004**, *104*, 5085–5113; b) A. Gorgues, P. Hudhomme, M. Sallé, *Chem. Rev.* **2004**, *104*, 5151–5184.
[6] a) M. Bendikov, F. Wudl, D. F. Perepichka, *Chem. Rev.* **2004**, *104*, 4891–4945; b) M. C. Diaz, B. M. Illescas, N. Martin, I. F. Perepichka, M. R. Bryce, E. Levillain, R. Viruela, E. Orti, *Chem. Eur. J.* **2006**, *12*, 2709–2721.
[7] a) F. Dumur, N. Gautier, N. Gallego-Planas, Y. Sahin, E. Levillain, N. Mercier, P. Hudhomme, M. Masino, A. Girlando, V. Lloveras, J. Vidal-Gancedo, J. Veciana, C. Rovira, *J. Org. Chem.* **2004**, *69*, 2164–2177; b) I. Fuks-Janczarek, J. Luc, B. Sahraoui, F. Dumur, P. Hudhomme, J. Berdowski, I. V. Kityk, *J. Phys. Chem. B* **2005**, *109*, 10179–10183.
[8] C. Loosli, C. Y. Jia, S-X. Liu, M. Haas, M. Dias, E. Levillain, A. Neels, G. Labat, A. Hauser, S. Decurtins, *J. Org. Chem.* **2005**, *70*, 4988–4992.
[9] a) J. Rusanova, S. Decurtins, E. Rusanov, H. Stoeckli-Evans, S. Delahaye, A. Hauser, *J. Chem. Soc. Dalton Trans.* **2002**, 4318–4320; b) S. Ott, R. Faust, *Synthesis* **2005**, 3135–3139.
[10] a) M. Cusumano, M. L. Di Pietro, A. Giannetto, *Inorg. Chem.* **2006**, *45*, 230–235; b) A. E. Friedman, J.-C. Chambron, J.-P. Sauvage, N. J. Turro, J. K. Barton, *J. Am. Chem. Soc.* **1990**, *112*, 4960–4962; c) R. M. Hartshorn, J. K. Barton, *J. Am. Chem. Soc.* **1992**, *114*, 5919–5925; d) C. Hiort, P. Lincoln, B. Nordén, *J. Am. Chem. Soc.* **1993**, *115*, 3448–3454.
[11] a) Y. Liu, A. Chouai, N. N. Degtyareva, D. A. Lutterman, K. R. Dunbar, C. Turro, *J. Am. Chem. Soc.* **2005**, *127*, 10796–10797; b) E. D. A. Stemp, M. R. Arkin, J. K. Barton, *J. Am. Chem. Soc.* **1995**, *117*, 2375–2376; c) C. G. Coates, L. Jacquet, J. J. McGarvey, S. E. J. Bell, A. H. R. Al-Obaidi, J. M. Kelly, *J. Am. Chem. Soc.* **1997**, *119*, 7130–7136.
[12] D. A. McGovern, A. Selmi, J. E. O'Brien, J. M. Kelly, C. Long, *Chem. Commun.* **2005**, 1402–1404.

[13] H. Meier, *Angew. Chem.* **2005**, *117*, 2536–2561; *Angew. Chem. Int. Ed.* **2005**, *44*, 2482–2506.
[14] J. A. Marsden, J. J. Miller, L. D. Shirtcliff, M. M. Haley, *J. Am. Chem. Soc.* **2005**, *127*, 2464–2476.
[15] D. M. Guldi, F. Giacalone, G. de la Torre, J. L. Segura, N. Martin, *Chem. Eur. J.* **2005**, *11*, 7199–7210.
[16] T. Michinobu, J. C. May, J. H. Lim, C. Boudon, J. P. Gisselbrecht, P. Seiler, M. Gross, I. Biaggio, F. Diederich, *Chem. Commun.* **2005**, 737–739.
[17] A. L. Thompson, T. S. Ahn, K. R. J. Thomas, S. Thayumanavan, T. J. Martinez, C. J. Bardeen, *J. Am. Chem. Soc.* **2005**, *127*, 16348–16349.
[18] A. L. Spek, *J. Appl. Crystallogr.* **2003**, *36*, 7–13.
[19] a) S. Bouguessa, A. K. Gouasmia, S. Golhen, L. Ouahab, J. M. Fabre, *Tetrahedron Lett.* **2003**, *44*, 9275–9278; b) S-X. Liu, S. Dolder, E. B. Rusanov, H. Stoeckli-Evans, S. Decurtins, *C. R. Acad. Sci. Paris, Chimie* **2003**, *6*, 657–662; c) T. Devic, N. Avarvari, P. Batail, *Chem. Eur. J.* **2004**, *10*, 3697–3707.
[20] T. K. Schoch, J. L. Hubbard, C. R. Zoch, G.-B. Yi, M. Sorlie, *Inorg. Chem.* **1996**, *35*, 4383–4390.
[21] J. L. Segura, N. Martín, *Angew. Chem.* **2001**, *113*, 1416–1455; *Angew. Chem. Int. Ed.* **2001**, *40*, 1372–1409.
[22] S. Sumalekshmy, K. R. Gopidas, *J. Phys. Chem. B* **2004**, *108*, 3705–3712.
[23] N. Mataga, Y. Kaifu, M. Koizumi, *Bull. Chem. Soc. Jpn.* **1956**, *29*, 465–470.
[24] X. Y. Lauteslager, I. H. M. van Stokkum, H. J. van Ramesdonk, D. Bebelaar, J. Fraanje, K. Goubitz, H. Schenk, A. M. Brouwer, J. W. Verhoeven, *Eur. J. Org. Chem.* **2001**, 3105–3118.
[25] a) R. Pou-Amérigo, E. Orti, M. Merchan, M. Rubio, P. M. Viruela, *J. Phys. Chem. A* **2002**, *106*, 631–640; b) R. Pou-Amérigo, P. M. Viruela, R. Viruela, M. Rubio, E. Orti, *Chem. Phys. Lett.* **2002**, *352*, 491–498.
[26] J. Fees, W. Kaim, M. Moscherosch, W. Matheis, J. Klima, M. Krejcik, S. Zalis, *Inorg. Chem.* **1993**, *32*, 166–174.
[27] C-Y. Jia, S-X. Liu, C. Tanner, C. Leiggener, L. Sanguinet, E. Levillain, S. Leutwyler, A. Hauser, S. Decurtins, *Chem. Commun.* **2006**, 1878–1880.
[28] J. L. Brusso, O. P. Clements, R. C. Haddon, M. E. Itkis, A. A. Leitch, R. T. Oakley, R. W. Reed, J. F. Richardson, *J. Am. Chem. Soc.* **2004**, *126*, 8256–8265.
[29] a) J. A. Hansen, J. Becher, J. O. Jeppesen, E. Levillain, M. B. Nielsen, B. M. Petersen, J. C. Petersen, Y. Sahin, *J. Mater. Chem.* **2004**, *14*, 179–184; b) N. Svenstrup, K. M. Rasmussen, T. Kruse Hansen, J. Becher, *Synthesis* **1994**, 809–812.
[30] a) W. Paw, R. Eisenberg, *Inorg. Chem.* **1997**, *36*, 2287–2293; b) G. F. Smith, F. W. Cagle, Jr., *J. Org. Chem.* **1947**, *12*, 781–784.
[31] Gaussian 03, Revision C.02, M. J. Frisch, G. W. Trucks, H. B. Schlegel, G. E. Scuseria, M. A. Robb, J. R. Cheeseman, J. A. Montgomery, Jr., T. Vreven, K. N. Kudin, J. C. Burant, J. M. Millam, S. S. Iyengar, J. Tomasi, V. Barone, B. Mennucci, M. Cossi, G. Scalmani, N. Rega, G. A. Petersson, H. Nakatsuji, M. Hada, M. Ehara, K. Toyota, R. Fukuda, J. Hasegawa, M. Ishida, T. Nakajima, Y. Honda, O. Kitao, H. Nakai, M. Klene, X. Li, J. E. Knox, H. P. Hratchian, J. B. Cross, V. Bakken, C. Adamo, J. Jaramillo, R. Gomperts, R. E. Stratmann, O. Yazyev, A. J. Austin, R. Cammi, C. Pomelli, J. W. Ochterski, P. Y. Ayala, K. Morokuma, G. A. Voth, P. Salvador, J. J. Dannenberg, V. G. Zakrzewski, S. Dapprich, A. D. Daniels, M. C. Strain, O. Farkas, D. K. Malick, A. D. Rabuck, K. Raghavachari, J. B. Foresman, J. V. Ortiz, Q. Cui, A. G. Baboul, S. Clifford, J. Cioslowski, B. B. Stefanov, G. Liu, A. Liashenko, P. Piskorz, I. Komaromi, R. L. Martin, D. J. Fox, T. Keith, M. A. Al-Laham, C. Y. Peng, A. Nanayakkara, M. Challacombe, P. M. W. Gill, B. Johnson, W. Chen, M. W. Wong, C. Gonzalez, J. A. Pople, Gaussian, Inc., Wallingford CT, **2004**.
[32] M. Frei, F. Diederich, *Helv. Chim. Acta* **2006**, *89*, 2040–2057.
[33] G. M. Sheldrick, *Acta Crystallogr. Sect. A* **1990**, *46*, 467–473.
[34] G. M. Sheldrick, SHELXL-97, Program for crystal structure refinement, University of Göttingen: Göttingen, Germany, **1997**.

Received: November 1, 2006
Published online: February 1, 2007

